The Astrophysical Journal, 994:229 (8pp), 2025 December 1 https://doi.org/10.3847/1538-4357/ae13e1

Survival of the Accretion Disk in LMC Recurrent Nova 1968-12a: UV–X-Ray Case Study of the 2024 Eruption

Judhajeet Basu[1,2], G.C. Anupama[1], Jan-Uwe Ness[3], Kulinder Pal Singh[4], Sudhanshu Barway[1], and Shatakshi Chamoli[1,2]
[1] Indian Institute of Astrophysics, II Block, Koramangala, Bengaluru 560034, India; judhajeet20@gmail.com
[2] Pondicherry University, R.V. Nagar, Kalapet, Pondicherry 605014, India
[3] European Space Agency, European Space Astronomy Centre, E-28692 Madrid, Spain
[4] Department of Physical Sciences, Indian Institute of Science Education and Research Mohali, 140306, Punjab, India
Received 2025 June 30; revised 2025 September 29; accepted 2025 October 12; published 2025 November 27

Abstract

We report on UV and X-ray observations of the 2024 eruption of the recurrent nova LMCN 1968-12a, a rapidly recurring extragalactic system with a ∼4.3 yr recurrence period and a massive white dwarf. The eruption was discovered on 2024 August 1.8 by Swift, and subsequently monitored using AstroSat's UVIT and Soft X-Ray Telescope, along with Swift's UVOT and X-Ray Telescope. The multiwavelength light curves reveal a rapid UV–optical decline, followed by a plateau phase exhibiting 1.26 day modulations consistent with the orbital period. The supersoft X-ray emission, which emerged by day 5, exhibited a double peak, suggesting variable obscuration that could be due to an inhomogeneous nova ejecta or due to a nova superremnant along the line of sight. Time-resolved X-ray spectroscopy shows a blackbody component with $T \approx 10^6$ K. The spectral energy distributions obtained concurrently in the UV, peaking at $T \approx 20{,}000$ K and with a source radius ∼2–3 $R_\odot$, are inconsistent with emission from the secondary star or nova photosphere alone. Instead, the UV emission is attributed to an irradiated accretion disk that survived the eruption. The persistent UV plateau and its temperature suggest that the accretion disk was not completely disrupted and resumed activity within days, consistent with recent findings in other rapidly recurring novae such as U Sco and M31N 2008-12a.

Unified Astronomy Thesaurus concepts: Cataclysmic variable stars (203); Recurrent novae (1366); Novae (1127); Ultraviolet astronomy (1736); X-ray astronomy (1810); Accretion (14); Binary stars (154); Eclipsing binary stars (444); Large Magellanic Cloud (903)

Materials only available in the online version of record: data behind figure

1. Introduction

Stars are often found in binary systems. When such a binary consists of a white dwarf (WD) and a main-sequence or a red/subgiant star, it can evolve into a close-binary cataclysmic variable system (R. P. Kraft 1964). Under these circumstances, the WD can accrete matter from the secondary star via a Roche-lobe overflow or winds from the secondary, forming an accretion disk. As the base of the accretion disk becomes denser and hotter (nearing Fermi temperature), the critical limits of thermonuclear runaway (TNR) are reached (D. M. Townsley & L. Bildsten 2004; S. Starrfield et al. 2016 and references therein). What follows is the release of energy ($\approx 10^{45}$ erg) and matter (at $v \gtrapprox 500$ km s^{-1}) from the system, known as a nova eruption (S. Starrfield et al. 2016). These transients are important sites for studying various physical processes such as TNRs, shock interactions, mass loss mechanisms, and galactic chemical enrichment (S. Starrfield et al. 2020; L. Chomiuk et al. 2021).

While it is known that an accretion disk is present at late times in old novae (P. Selvelli & R. Gilmozzi 2013; J. Basu et al. 2024a; G. Sala et al. 2025), there is no consensus on the level of damage to the accretion disk during the outburst. It might remain intact in part (or completely, though this is less likely) within the optically thick ejecta. As the photosphere recedes toward the WD and the ejected material becomes transparent, the (surviving) disk may become visible once more. Accretion resumes and the cycle of nova eruptions repeats after a time interval that depends on the WD mass, the accretion rate, and the nature of the secondary (M. M. Shara et al. 2018; Y. Hillman et al. 2020). Systems that have exhibited multiple nova eruptions within timescales of decades or less are classified as recurrent novae (RNe), that is, novae with more than one observed outburst from the same system. In contrast, systems with much longer recurrence timescales, such that only a single eruption has been observed, are termed classical novae (CNe).

High WD mass and accretion rate drive rapid RNe. Earlier models by S. G. Starrfield et al. (1975), M. Kato et al. (2014), and S. Starrfield et al. (2016) predicted these systems required massive WDs. M. M. Shara et al. (2018) built upon and validated these predictions, confirming massive WDs for RNe. The shorter the recurrence period, the more massive the WD is. Hence, such systems that contain a CO WD (thus not too rich in α elements) are also top contenders for Type Ia supernova progenitors (Y. Hillman et al. 2016; B. Wang 2018).

LMC recurrent nova 1968-12a (hereafter LMCN 1968-12a) was the first extragalactic RN to be discovered in 1968. It has erupted several times since then (see Table 1). Recent eruptions reveal a recurrence period of roughly 4.3 yr. This is shorter than the recurrence period for any Galactic recurrent nova and longer than only two other extragalactic novae,

Table 1
List of All Previous Known Eruptions of LMCN 1968-12a

Discovery			Eruption Date	Time Since Last Eruption	SSS t_{off} date	References
UT	(mag)	Filter	(MJD)	(days)	(days)	
1968 Dec 16.5	10.9	m_{pg}	40206.0 ± 1.5	⋯	⋯	(1)
⋮						
1990 Feb 14.1	11.2	m_{pv}	47936.1 ± ?	⋯	⋯	(2)
⋮						
2002 Oct 10	11.15 ± 0.02	V	52557.3 ± 1.0	⋯	⋯	(3, 4)
⋮						
2010 Nov 21.2	11.7 ± 0.3	I	55521.2 ± 1.0	⋯	⋯	(5)
2016 Jan 21.2	11.5 ± 0.2	I	57407.4 ± 0.8	1886.2 ± 1.8	56.1	(4)
2020 May 06.7	13.99 ± 0.08	g	58971.9 ± 0.4	1564.5 ± 1.2	60	(6, 7)[a]
2024 Aug 01.8	9.9 ± 0.1	$uvm2$	60523.5 ± 0.3	1551.6 ± 0.7	> 50	(8), this work

Notes. The vertical dots in the Discovery (UT) column represent eruption(s) which were likely missed or not detected.
[a] https://www.aavso.org/lmc-v1341-new-recurrent-nova-eruption
References. (1) J. Sievers (1970), (2) W. Liller (1990), (3) G. Pojmanski (2002), (4) N. P. M. Kuin et al. (2020), (5) P. Mróz et al. (2014), (6) K. L. Page et al. (2020), (7) G. J. Schwarz et al. (2020), (8) M. J. Darnley et al. (2024).

M31N 2008-12a (M. J. Darnley et al. 2016; M. Henze et al. 2018; J. Basu et al. 2024b) and M31N 2017-01e (A. W. Shafter et al. 2022, 2024; S. Chamoli et al. 2025). It falls in the category of rapidly recurring systems that have massive WDs (M. J. Darnley 2021). Previous studies of past eruptions of this system concluded that the WD in this binary is >1.3 $M_{\odot}$, it has an orbital period of 1.26 days, and the mass of the ejecta was comparable to that of the accreted mass (N. P. M. Kuin et al. 2020).

The most recent outburst of LMCN 1968-12a was discovered on 2024 August 1.8 UT by the Swift observatory. The last quiescent detection was on 2024 August 1.19 UT in the *UVW*1 filter at 18.19 ± 0.09 mag (M. J. Darnley et al. 2024). The eruption time, estimated to be the midpoint of these two times, is given in Table 1. This has been used as the reference time throughout this work.

In this paper, we present the UV and X-ray observations of the 2024 outburst based on data obtained with AstroSat's Ultraviolet Imaging Telescope (UVIT) and Soft X-Ray Telescope (SXT), combined with data from Swift's UV/Optical Telescope (UVOT) and X-Ray Telescope (XRT).

2. Observations and Data

M. J. Darnley et al. (2024) reported the 2024 eruption of the RN on 2024 August 1, when it was observed to brighten by more than 8 mag in ∼ 15 hr during the monthly monitoring of the RN field by Swift. Soon, it was followed up in UV and X-ray wave bands by both AstroSat and Swift, as discussed below.

2.1. AstroSat

AstroSat (K. P. Singh et al. 2014) is a space-based observatory carrying three imaging telescopes: two UVITs, one for the near-UV (NUV) and the other for the far-UV (FUV) channel (S. N. Tandon et al. 2017), and SXT (K. P. Singh et al. 2017). Each UVIT telescope has a primary diameter of 37.5 cm with a field of view of 28′. Both the NUV and FUV have multiple filters (S. N. Tandon et al. 2017). We used only the FUV channel with F148W and F172M filters. The NUV channel was not available. UVIT has a spatial resolution of around 1.″5. In soft X-rays, SXT can observe in the 0.3–7 keV range with a spectral resolution of about 90–130 eV and a spatial resolution of 4′. We utilized channels in the 0.3–2 keV range, which is suitable for studying the supersoft source phase of novae (S. Bhattacharyya et al. 2021).

After the discovery, we submitted a target of opportunity (ToO) proposal for AstroSat UV and soft X-ray observations of LMCN 1968-12a. The first set of observations was performed on 2024 August 15, 14 days after the outburst (Epoch I). It involved two orbits of UVIT observations: one using the F148W filter with an exposure of around 180 s and another using the F172M filter with an exposure of around 760 s. Simultaneously, SXT observed the object with a total effective exposure time of around 6600 s. A second ToO proposal was submitted to obtain a deep exposure during the supersoft phase, resulting in AstroSat observations of the object again on 2024 August 20–21 (Epoch II). It included 16 orbits of UVIT observations, amounting to 12.6 ks of useful exposure with the F148W filter. The corresponding useful SXT exposure time was 23.2 ks, from all orbits.

The UVIT L1 data were downloaded from the AstroSat archive and processed using the `CCDLAB` software (J. E. Postma & D. Leahy 2021) to obtain the L2 data. Adhering to the steps in J. Basu et al. (2024a), point-spread function (PSF) photometry was performed, followed by aperture correction derived from bright stars and zero-point corrections taken from S. N. Tandon et al. (2020). For spectral energy distribution (SED) analysis, UV magnitudes were dereddened by $E(B-V) = 0.07 \pm 0.01$, taken from the previous study (N. P. M. Kuin et al. 2020).

Orbit-wise SXT data were downloaded from the AstroSat archive and merged together with the `SXTMerger` package in `JULIA`. The SXT data were binned at 3000 s to generate light curves with an optimum signal-to-noise ratio using `xselect (v2.4m)` in `HEASoft`. SXT spectra were extracted from orbit-wise, cleaned event files using `xspec (v12.12.0)`. A circular region of 12′ and an annulus of 15′–17′ radius were chosen as the source and background region, respectively, to extract the counts. The latest available Ancillary Response Files (ARF) and Response Matrix Files (RMF) were used for the analysis of spectra. The spectral analysis involved Poisson statistics (cstat), interstellar medium (ISM) abundances given in J. Wilms et al. (2000), and the Tübingen–Boulder (`tbabs`) ISM absorption model to account for neutral H in the

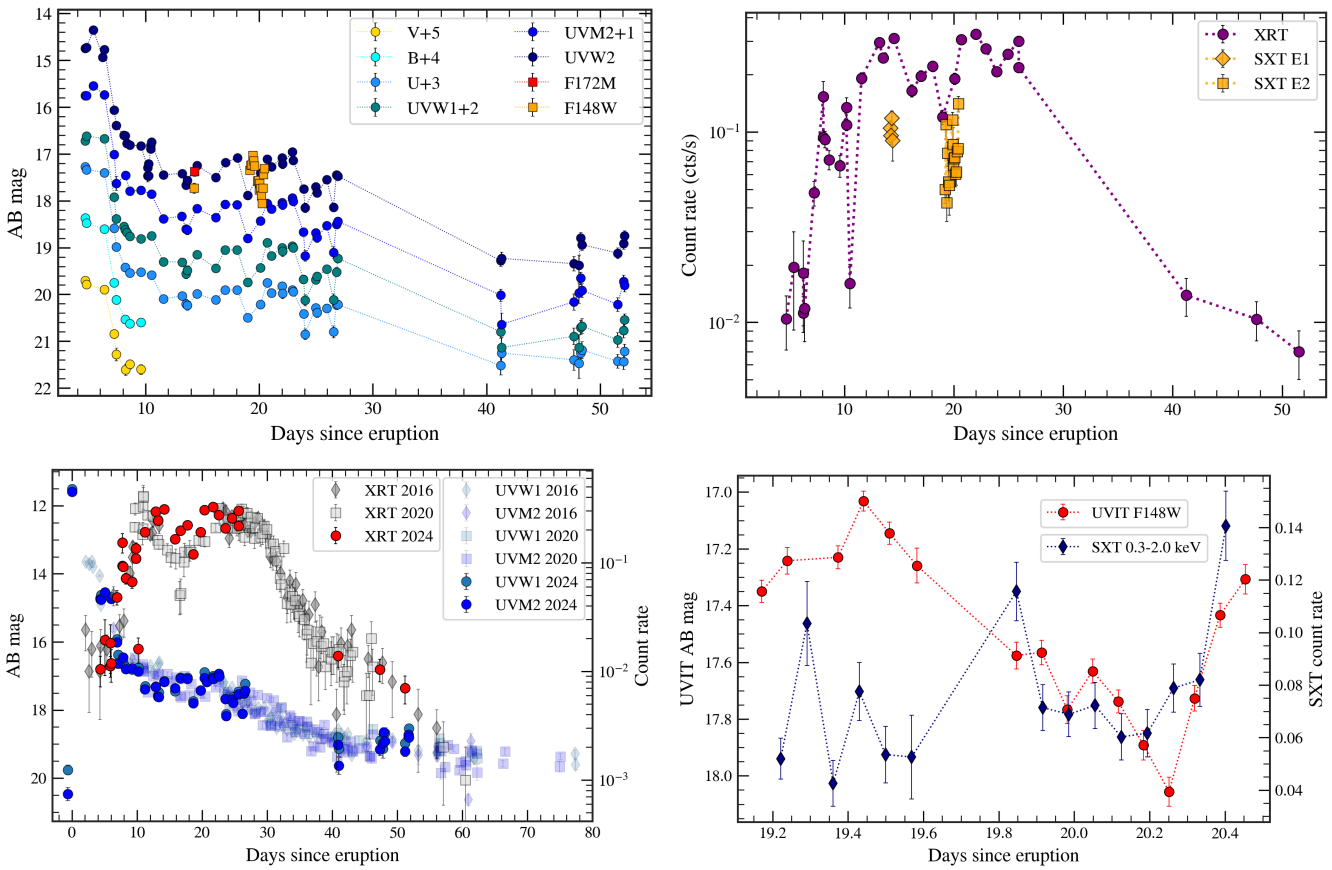

Figure 1. UV and X-ray light curves of LMCN 1968-12a. Top: UV (left) and X-ray (right) light curves of the 2024 eruption of LMCN 1968-12a. Bottom left: UV and X-ray light curves of the 2024 eruption overplotted on the light curves of previous eruptions. Bottom right: zoomed-in view of the second epoch of AstroSat observations, showing variability consistent with a 1.26 day period, though only a single cycle is covered. The 2024 eruption data are available in machine readable format.

(The data used to create this figure are available in the online article.)

intervening medium. Here, we assume $N_{\rm H} = 1.8 \times 10^{21}$ cm^{-2}, which is the column density of the ISM and has been shown to be undisturbed by the optical depth of the ejecta after 10 days from eruption by N. P. M. Kuin et al. (2020).

The UV and X-ray light curves are shown in Figure 1, and some of the X-ray spectra are shown in Figure 2.

2.2. *Swift*

Swift (N. Gehrels et al. 2004) consists of UVOT (P. W. A. Roming et al. 2005) and XRT (D. N. Burrows et al. 2005). UVOT has a spatial resolution of 2.″3, whereas XRT has a spatial resolution of 18″ and a spectral resolution similar to that of SXT. Swift monitored the object every month to look for any new outbursts. As soon as the 2024 outburst was detected (M. J. Darnley et al. 2024), Swift started daily monitoring from 2024 August 1, which lasted up to August 28 with both UVOT and XRT. It pointed to the object again on September 11, 18, and 22 after a gap of almost two weeks due to observational constraints. Publicly available L2 data were downloaded from the Swift archives.

UVOT data were analyzed using the `uvotmaghist (v1.3)` command in `HEASoft`. A source region of 5″ centered at the source was used for aperture photometry, and a similar aperture in a source-free region near the nova was used to estimate the background. UVOT observations included *V*, *B*, *U*, *UVW*1, *UVM*2, and *UVW*2 filters. Observations using *B* and *V* filters are restricted to the first 10 days, whereas complete light curves are available for the other filters, shown in Figure 1.

XRT data were analyzed using the `ximage/sosta (v4.5.1)` package within `HEASoft`, which corrects the counts for vignetting, dead time loss, background subtraction, and the PSF of the instrument. ARF was generated from the exposure maps to extract the spectra, while RMF was taken from the calibration database. Other parameters used in `xspec` were kept the same as for the SXT spectra analysis. The XRT light curve and a couple of XRT spectra are shown in Figure 1 and Figure 2, respectively. The temperature and $N_{\rm H}$ were also independently determined from the XRT spectra, and their evolution is displayed in Figure 3. The `error` command was used to determine the 68% and 90% confidence intervals for these parameters. $N_{\rm H}$ at > 12 days from eruption was found to be largely consistent with the previous results obtained by N. P. M. Kuin et al. (2020).

The AstroSat and Swift data are available in the form of machine readable tables as described in Figure 1.

3. Results

3.1. *Light Curves*

Days 0–8. LMCN 1968-12a reached its maximum magnitude of 9.9 $\pm$ 0.1 on 2024 August 1.83 in the *UVM*2 filter

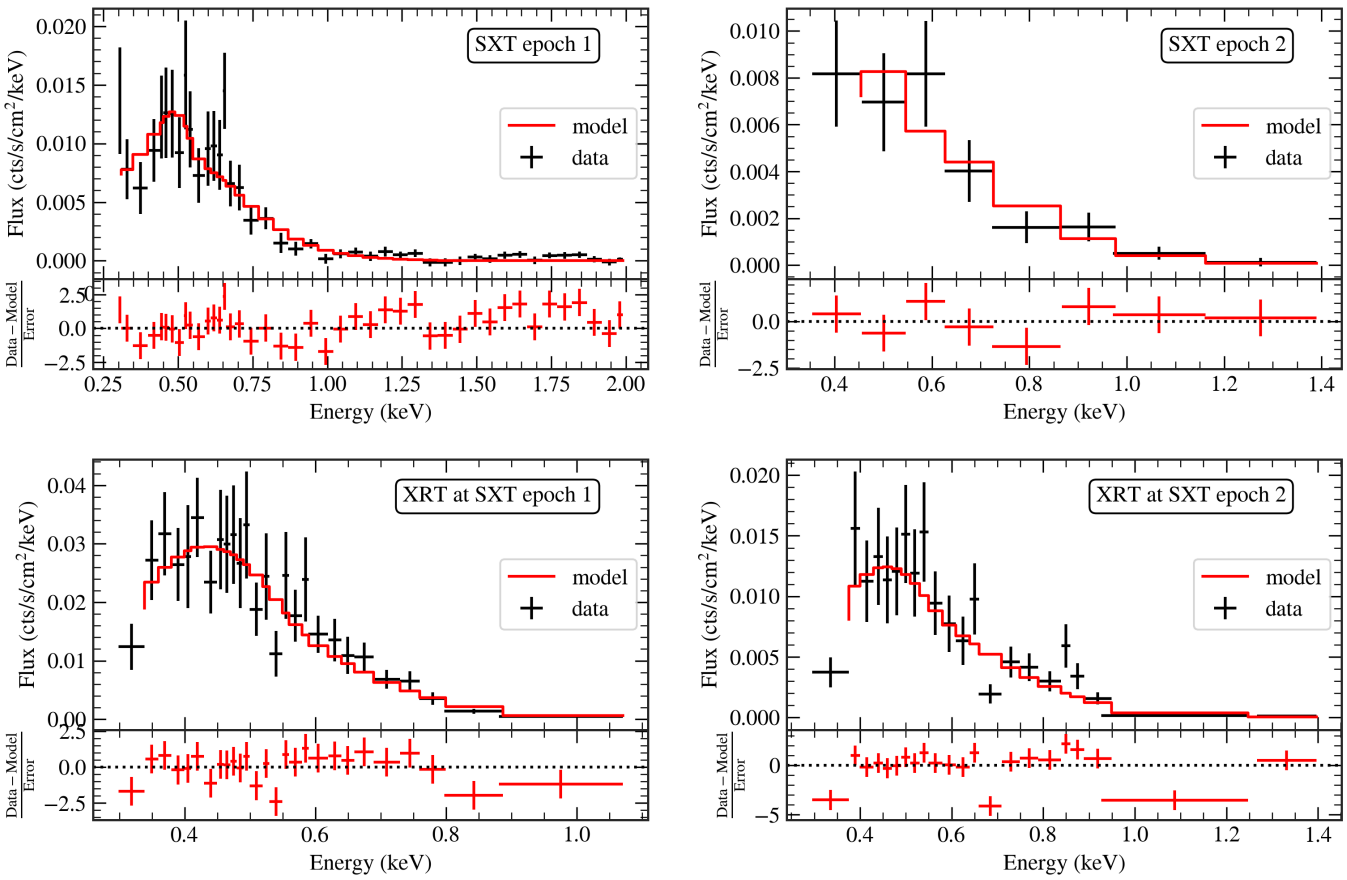

Figure 2. Top panel: AstroSat/SXT spectra observed at Epoch I (2024 August 15 16:19–22:35 UT; $t_{exp} \approx 100$ minutes) and Epoch II (2024 August 21 14:28-14:58 UT; $t_{exp} \approx 30$ minutes). Bottom panel: Swift/XRT spectra on 2024 August 16 00:23-00:45 UT ($t_{exp} \approx 22$ minutes) and August 21 14:14–14:36 UT ($t_{exp} \approx 22$ minutes), at epochs close to the AstroSat observations. Best-fit `tbabs × bb` models are shown in red. The fit residuals are also shown for each subplot. The best-fit parameters are given in Section 4.2.

(M. J. Darnley et al. 2024). The UV and optical light curves follow a steep decline up to day 8 from the peak of the eruption, as shown in Figure 1. The rapid decline rate during this phase is ∼0.8 mag day^{-1} in all UVOT filters. The soft X-ray flux emerged during this UV-decline phase around day 5, and increased from the detection limit (0.014 counts s^{-1}) to more than 0.05 counts s^{-1} in the XRT bands.

Days 8–24. Modulations with a period of ∼1.3 days are observed in all UV bands during this phase and are attributed to the orbital period (N. P. M. Kuin et al. 2020). The high-cadence UVIT data around day 20 show evidence consistent with the 1.26 day orbital period, although the observations span only a single cycle, as illustrated in the bottom-right panel of Figure 1. N. P. M. Kuin et al. (2020) observed that the eclipse duration is only 0.05 parts of a full phase. Some UVOT data points, such as those on days 19 and 24, show significant dips in the light curve. The UVIT *F*148*W* flux also shows a dip between days 19.8 and 20.4 (AstroSat Epoch II).

The peaks of these light-curve modulations in the UV bands show a gradual decline of 1 mag in 16 days (see the top-left panel in Figure 1), representing the plateau phase, which is often seen in RNe (A. Pagnotta & B. E. Schaefer 2014). The UV light curve during the plateau phase is very similar to the one seen in U Sco, a Galactic RN with a similar orbital period and a slightly longer recurrence period (A. Evans et al. 2023; K. Muraoka et al. 2024).

Another common feature observed during the plateau phase is the rise to the maximum of supersoft source (SSS) emission, originating from the WD's surface. As shown in Figure 1, the XRT count rate increases and reaches a peak flux of 0.3 counts s^{-1} during this phase. The SXT count rates, known to be approximately 0.3 times the XRT count rates (owing to lower sensitivity), follow the XRT light curve. Similar to the UV light curve, the SSS light curve also shows orbital modulations. Additionally, the SSS light curve has a double-peaked structure with a decrease in the flux during days ∼16–20. Similar features were seen in the previous outbursts, with the broad inflection being more prominent, as shown in the lower-left panel of Figure 1. The Epoch II AstroSat-SXT observations indicate a sharp dip during days 19.8 and 20.4 (bottom-right plot in Figure 1), which is more akin to the orbital modulation.

3.2. X-Ray Spectroscopy

SXT spectra were obtained during both Epoch I (around day 15) and Epoch II (around day 20). For Epoch I, spectra from all four orbits were combined, as their count rates were consistent within the uncertainties, and the merged spectrum is shown in Figure 2. In contrast, the deeper Epoch II exhibits significant variability (see Figure 1). Therefore, only the spectrum from the orbit closest in time to an XRT observation is presented in Figure 2. From the light curve in Figure 1, it is

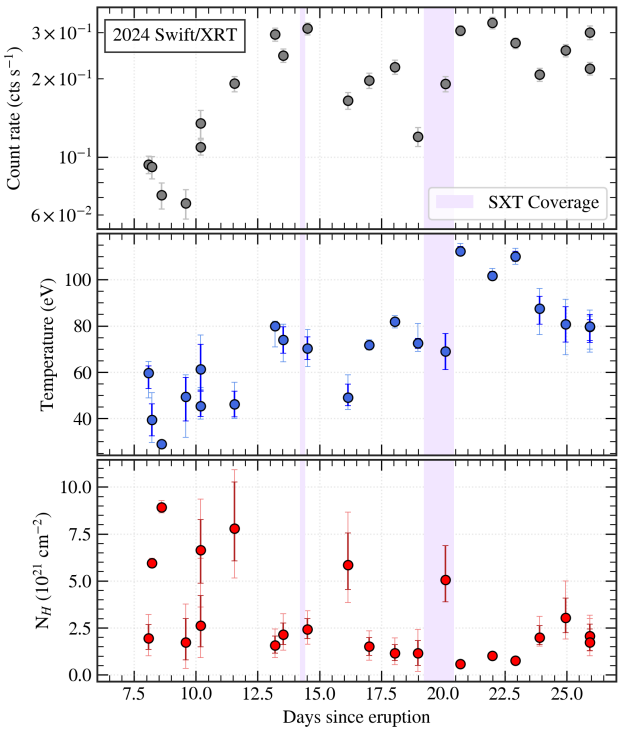

Figure 3. The XRT light curve of the 2024 eruption is shown in the top panel. Evolution of the supersoft blackbody temperature and $N_{\rm H}$ are plotted in the middle and bottom panels, respectively. The 68% and 90% confidence intervals for temperature and $N_{\rm H}$ are also shown.

evident that both epochs occurred during the peak of the supersoft phase. In Epoch I, the spectral evolution suggests that most of the radiation is below 1 keV, owing to its supersoft nature. During Epoch II as well, most of the counts are concentrated below 1 keV, with almost no photons above 1.5 keV. The dense temporal evolution during the second epoch shows highly variable spectra during the supersoft phase. The flux density rises almost 5 times and declines back to the initial level in 4–5 hr during this epoch of observation. Toward the end of the observation of Epoch II, the 0.3–1.0 keV flux starts to rise again. These variabilities are also evident from the X-ray light curves shown in Figure 1. The high variability of SSS emission below 1 keV lasting over timescales of hours is discussed in Section 4.1. Although the spectral evolution hints at transient features consistent with lines seen during the SSS phase in novae (M. Orio et al. 2020; J. U. Ness et al. 2022), the limited resolution of the X-ray data in this case limits any noteworthy interpretation.

Nonetheless, these X-ray spectra are still useful for deriving physical parameters of the source region, close to the surface of the WD. The X-ray spectra from the two individual SXT epochs and their corresponding nearest XRT spectra are shown in Figure 2. These X-ray spectra were modeled with blackbody functions for their simplicity and reproducibility. It should be noted that blackbody fits are not physically accurate representations of the WD's atmosphere. But, given the limited spectral resolution of the data, it still provides a reasonable approximation of key parameters such as the effective temperature of the surface of the WD photosphere. The observed data points, together with the corresponding best-fit models and the residuals, are also shown in Figure 2. For the AstroSat-SXT data, the best-fit temperatures during Epochs I and II are of order $\sim 10^6$ K. It is consistent with the near-simultaneous Swift/XRT measurements as shown in Figure 4. Extending this analysis to all the XRT data due to their good cadence throughout the SSS phase, we could obtain the temporal change of the effective temperature and the neutral hydrogen column density. This evolution is shown in Figure 3. We notice that the rise and drop in X-ray flux corresponds to similar behavior in the temperature as well. The $N_{\rm H}$, on the other hand, stabilizes around 1.5×10^{21} cm^{-2} after day 13, which was also reported by N. P. M. Kuin et al. (2020) for the 2016 eruption. It is consistent with the ISM $N_{\rm H}$ values derived from other sources. However, it is interesting to note that $N_{\rm H}$ shows an increase in a couple of instances corresponding to a drop in the flux and temperature. This behavior has been explored in Section 4.1.

4. Discussion

4.1. The Double-peaked Nature of the X-Ray Light Curve

The rise of the SSS emission is due to the ejecta becoming optically thin while expanding (J. Krautter et al. 1996). This is evident from the drop in the column density noticed in Figure 3. The expanding ejecta reveals the X-ray photons originating from deeper layers near the surface of the WD. The origin of UV photons, however, is debated.

It was noted in Section 3.1 that on days 19 and 24, the UV flux drops sharply in all the UVOT filters. By overplotting the eclipse durations on the flux evolution in Figure 4, we notice that these dips are actually caused by the eclipsing of the WD by the secondary. Since the UV light curve shows eclipses, it must have been emitted from somewhere within the orbit of the secondary. The simultaneous drop in UV–X-ray flux during day 19.8–20.4 noticed in the high-cadence AstroSat Epoch II observations (bottom-right plot in Figure 1) must also be because of the secondary star eclipsing the WD and the disk. As the WD emerges from behind the secondary, the UV–X-ray fluxes start to rise again after day 20.6. However, this dip around day 20 is not related to the overall wide drop in the SSS light curve observed between days 16–20. The timescale and intensity of the broader drop, revealing the light curve as a double-humped peak, differ from those attributed to orbital modulation. Consequently, it is reasonable to assume that orbital motion is not a cause of the double-humped SSS peak.

Double-humped SSS emission, along with high variability, has been observed in other well-studied RNe. V3890 Sgr displayed a highly variable X-ray light curve, featuring dips on timescales ranging from hours to days (K. P. Singh et al. 2021; J. U. Ness et al. 2022). The hourly dips were attributed by J. U. Ness et al. (2022) to clumps of ejecta orbiting within the system at radii of 5–150 $R_{\rm WD}$. In contrast, an extended low-flux interval from day 16.8–17.8, or a "faint X-ray episode," was probably caused by a sudden outflow of matter (K. P. Singh et al. 2021). This outflow was hypothesized to be partially opaque to X-rays but with a low filling factor, allowing the observed spectrum and column density ($N_{\rm H}$) to remain largely unaffected, though $N_{\rm H}$ estimation was limited by low signal-to-noise ratio. In particular, this episode lacked the short-term variability seen at other times.

RS Oph exhibited diverse variability during its 2006 and 2021 eruptions. J. P. Osborne et al. (2011) reported high-amplitude variations on timescales of tens of hours during the rise of the SSS phase in 2006, attributed to variable absorption

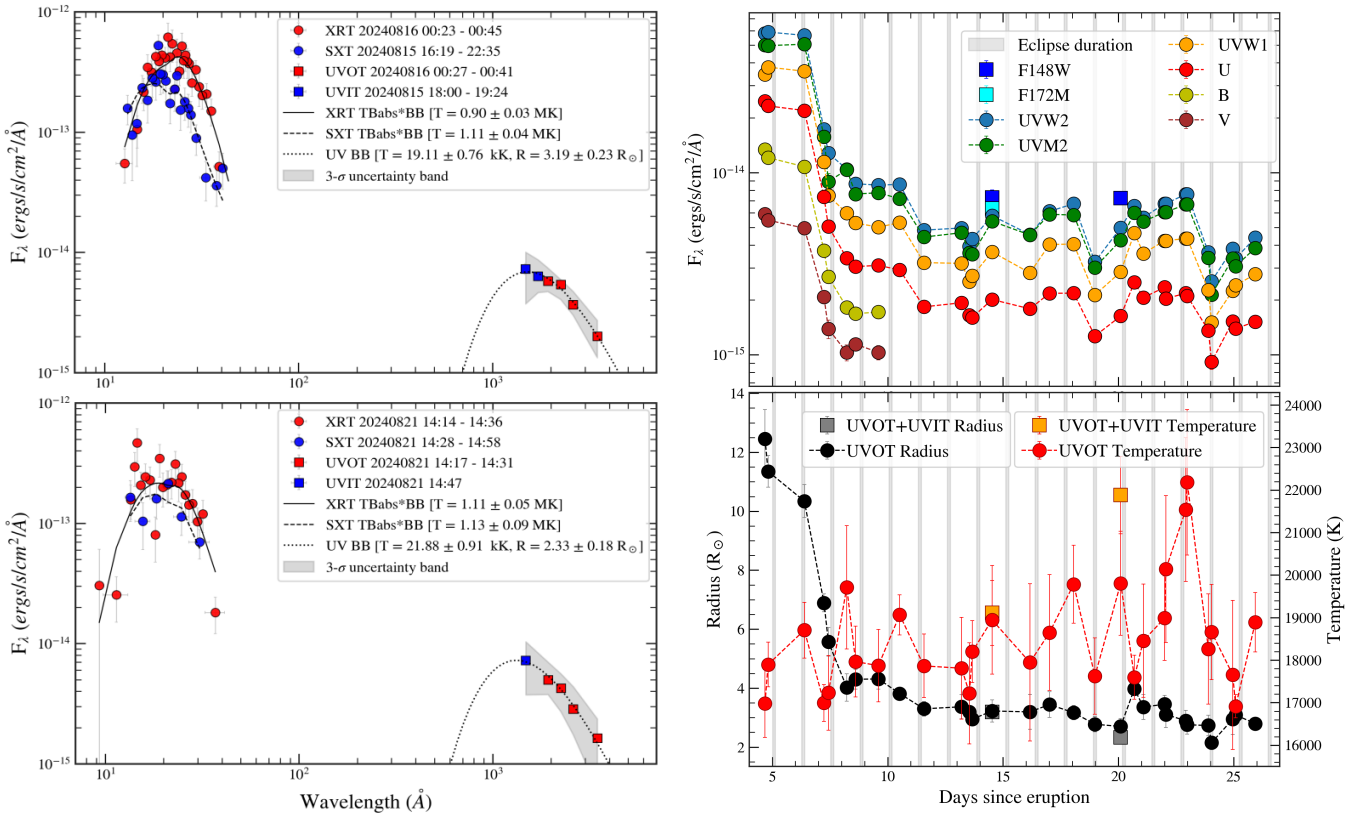

Figure 4. Left: blackbody fits to the X-ray (SXT and XRT) and UV (UVIT and UVOT) data are overplotted on the observed spectra for Epoch I (top) and Epoch II (bottom); the corresponding best-fit parameters are listed in the legends. Right: the top panel shows the temporal evolution of the flux in different UV filters, while the bottom panel presents the evolution of the inferred model parameters, i.e., the radius and effective temperature of the UV-emitting source.

by clumpy ejecta. In comparison, the 2021 SSS light curve was fainter and displayed a multipeaked structure. J. U. Ness et al. (2023) proposed that these differences arise from varying optical depths due to inhomogeneous ejecta across different outbursts. Interestingly, the 2021 eruption also featured a broad dip in X-ray emission between days 47 and 57 (see Figure 1 in J. U. Ness et al. 2023), similar in duration to that seen in LMCN 1968-12a, though its origin remains unclear.

The soft X-ray light curve of U Sco during its 2010 eruption showed an initial rise followed by a plateau phase of nearly constant flux until day 20, before reaching its peak around day 30 (A. Pagnotta et al. 2015). Until day 25, it also exhibited sharp, aperiodic dips lasting several hours, attributed to occultations of the central source by dense absorbing material aligned with the trajectory of a reforming accretion stream (J. U. Ness et al. 2012). For the 2022 eruption, K. Muraoka et al. (2024) reported that the early X-ray emission was fainter than in 2010, probably due to a lower accreted mass and consequently a reduced posteruption envelope mass.

M31N 2008-12a has also shown high variability in X-rays (M. J. Darnley et al. 2016; M. Henze et al. 2018). Like LMCN 1968-12a, it also demonstrates a major dip near the midpoint of the SSS phase, consistently over almost all eruptions lasting more than a day (see Figure 7 in J. Basu et al. 2024b).

Short-timescale variability, lasting from several minutes to a few hours, is commonly attributed to clumpy ejecta or inhomogeneous structures such as reforming accretion streams, which obscure the WD photosphere. The depths and durations of these dips are expected to vary between eruptions. However, in systems like LMCN 1968-12a and M31N 2008-12a, the observed day-scale dips appear to be remarkably consistent across multiple eruptions. In particular, the double-peaked structure in the LMCN 1968-12a X-ray light curve (see bottom-left panel of Figure 1) is repeatedly observed in at least its two most recent eruptions. We probed the blackbody effective temperature (kT) and the neutral hydrogen column density ($N_{\rm H}$) from the XRT data of the supersoft phase in 2024 by fitting a simple `tbabs × bb` model, keeping all parameters free. As shown in Figure 3, the drop in flux between days 16 and 20 indicates a correlated drop in temperature. An interesting point to note is that $N_{\rm H}$ increases from the ISM value during the days corresponding to the decrease in the X-ray flux and temperature. Since the dip from day 16–20 is much wider than the usual faster timescale variability seen in the SSS phases of RNe, and occurs at the same phase during the two outbursts, it is unlikely to be caused by clumps in the ejecta. It is more likely to be caused by obscuration due to external inhomogeneous material.

Recent studies have found faint nebulosities around RNe M31N 2008-12a (M. J. Darnley et al. 2019), KT Eri (M. W. Healy-Kalesh et al. 2024b; M. M. Shara et al. 2024a), RS Oph (M. W. Healy-Kalesh et al. 2024a; M. M. Shara et al. 2025), and T CrB (M. M. Shara et al. 2024b) that are orders of magnitude larger than the usual nova shells. These substantially extended nebulosities, termed nova superremnants (M. W. Healy-Kalesh et al. 2023), are believed to be a result of ISM swept up by repeated nova eruptions. Such structures are expected to be more prominent in the case of RNe due to their multiple nova outbursts over thousands of years. The presence of such an extended, inhomogeneous structure along the line of sight could possibly explain the dips lasting for days

seen during the SSS phase in LMCN 1968-12a, and possibly M31N 2008-12a.

4.2. Signatures of the Surviving Accretion Disk

Simultaneous NUV, FUV, and X-ray observations with AstroSat and Swift motivated us to look into the SED of the evolving system. SEDs covering the X-ray–UV wave bands during AstroSat Epochs I and II are shown in Figure 4. It is evident that the soft X-ray and UV fluxes originate from different sources. A single blackbody fit to the combined X-ray and UV data did not yield a good fit, with the X-ray tail being much weaker in the UV wave bands than what the observations suggest. As a result, the X-ray and UV data were modeled separately. The X-ray component was fitted with a blackbody modified by an absorption column mentioned in Section 2, whereas the extinction-corrected UV component was fitted only with a blackbody model. The results for AstroSat Epochs I and II, combined with near-simultaneous Swift data, are shown in Figure 4. The X-ray component, which is responsible for the SSS phase, peaks at around 10^6 K, which was also reported by N. P. M. Kuin et al. (2020) and suggested to originate at the surface of the WD. Meanwhile, the UV component peaks at roughly 2×10^4 K and has a source size of 2–3 $R_\odot$ during these epochs (days $\sim$15 and $\sim$20).

The Swift UVOT data were also individually fitted with blackbodies to estimate the temporal variation in radius and temperature of the source, as shown in Figure 4 (bottom-right panel). The radius of the UV source decreases until day 8, which coincides with the beginning of the SSS phase. This decrease in radius from 12 to 4 $R_\odot$ traces the receding photosphere toward the WD surface, which subsequently gives rise to the SSS phase in X-rays and a plateau phase in UV–optical bands. During the SSS phase, the radius of the UV source stays nearly constant at roughly 3 $R_\odot$, while the temperature is estimated to be between 1.7 and 2.3 $\times$ 10^4 K, consistent with the results from A. Evans et al. (2025). The UV blackbody component cannot originate from the secondary evolved star or the accretion disk alone. However, if either or both of these are irradiated by the hot WD, having a temperature that peaks at 10^6 K, it can give rise to UV–optical blackbody radiation. N. P. M. Kuin et al. (2020) and A. Evans et al. (2025) ruled out the possibility of an irradiated secondary as the model predictions in such a case overestimate the observed UV–optical fluxes.

The survival of the accretion disk after a nova outburst has been debated over the years. Recent studies of rapid RNe such as M31N 2008-12a (J. Basu et al. 2024b) and U Sco (J. U. Ness et al. 2012; K. Muraoka et al. 2025) indicate that the disk is present during the supersoft phase, even if in a fragmented form due to the impact of the nova eruption. U Sco showed signatures of accretion stream as early as 8 days after eruption (G. C. Anupama et al. 2013). Recent simulations by J. Figueira et al. (2025) also support the disk survival scenario under certain circumstances for RNe like U Sco. Disk irradiance is not rare and has been suggested to be the case for the optical plateau in U Sco (K. Muraoka et al. 2024), an RN with a similar orbital period and the same order of recurrence period as LMCN 1968-12a. I. Hachisu et al. (2000) generated theoretical models of an irradiated disk and secondary for U Sco, which could reproduce its UV–optical light curve. It is more than likely that the same phenomenon is also responsible for LMCN 1968-12a, given the similarities between these two RNe.

The accretion disk therefore appears to survive the nova outburst in this case. RNe typically host very massive WDs, which require a smaller ignition mass to trigger an eruption. This, in turn, leads to a relatively low ejecta mass (A. J. Kemp et al. 2024). Under such conditions, the impact on the accretion disk is expected to be less severe than in CNe, increasing the likelihood of disk survival after eruption. A direct consequence is the rapid resumption of accretion in RNe, within timescales of the order of SSS t_{on}, which in turn alleviates their recurrent nature.

5. Conclusions

In this work, we have analyzed the UV–X-ray light curves along with X-ray spectra and UV SEDs of the 2024 eruption of LMCN 1968-12a, a nearby rapidly recurring nova with a massive WD. The UV light curves show an initial steep decline followed by a plateau phase, which is modulated by the orbital period. As the UV light curve declines, the photosphere recedes, and the X-ray emission becomes visible. During the SSS phase, the X-ray emission is variable and also shows a major dip across outbursts, which could be due to a large absorbing medium along the line of sight, such as a nova superremnant. The X-ray spectra and the UV SED modeling indicate that the X-ray and UV emission come from different regions. Soft X-rays are emitted by residual burning on the WD surface at a temperature of $\sim$$10^6$ K. At the same time, UV–optical emission is dominated by the irradiated accretion disk at a temperature of 2×10^4 K. It is therefore evident from this study and previous studies of rapidly recurring nova systems that the accretion disk is not fully disrupted and accretion resumes within days after eruption.

Acknowledgments

We would like to thank the anonymous referee for the valuable comments that improved the quality of this work.

This work uses the SXT and UVIT data from the AstroSat mission of the Indian Space Research Organisation (ISRO). We thank the AstroSat TAC for allowing us ToO time to observe this nova in 2024. We thank the SXT and UVIT payload operation centers for verifying and releasing the data via the ISSDC data archive and providing the necessary software tools. JB thanks Dr. Prajwel Joseph at UVIT POC for the discussions on UVIT data.

We acknowledge the use of public data from the Swift data archive. This work has also used software and/or web tools obtained from NASA's High Energy Astrophysics Science Archive Research Center (HEASARC), a service of the Goddard Space Flight Center and the Smithsonian Astrophysical Observatory.

K.P.S. and G.C.A. thank the Indian National Science Academy (INSA) for support under the INSA Senior Scientist Programme.

Facilities: AstroSat (UVIT and SXT), Swift (UVOT and XRT).

Software: `CCDLAB` (J. E. Postma & D. Leahy 2021), `IRAF v2.16.1` (D. Tody 1993), `HEASoft v6.29`, `ximage v4.5.1`, and `xselect v2.4m` (Nasa High Energy Astrophysics Science Archive Research Center (Heasarc) 2014), `xspec v12.12.0` (K. A. Arnaud 1996), `Python v3.8.17`

(G. Van Rossum & F. L. Drake 2009), `NumPy v1.24.4` (C. R. Harris et al. 2020), `pandas v1.5.3` (W. McKinney 2010), `matplotlib v3.7.1` (J. D. Hunter 2007), `astropy v5.0.6` (Astropy Collaboration et al. 2022).

ORCID iDs

Judhajeet Basu https://orcid.org/0000-0001-7570-545X
G.C. Anupama https://orcid.org/0000-0003-3533-7183
Jan-Uwe Ness https://orcid.org/0000-0003-0440-7193
Kulinder Pal Singh https://orcid.org/0000-0001-6952-3887
Sudhanshu Barway https://orcid.org/0000-0002-3927-5402
Shatakshi Chamoli https://orcid.org/0009-0000-5909-293X

References

Anupama, G. C., Kamath, U. S., Ramaprakash, A. N., et al. 2013, A&A, 559, A121
Arnaud, K. A. 1996, ASPC, 101, 17
Astropy Collaboration, Price-Whelan, A. M., Lim, P. L., et al. 2022, ApJ, 935, 167
Basu, J., Krishnendu, S., Barway, S., Chamoli, S., & Anupama, G. C. 2024a, ApJ, 971, 8
Basu, J., Pavana, M., Anupama, G. C., et al. 2024b, ApJ, 966, 44
Bhattacharyya, S., Singh, K. P., Stewart, G., et al. 2021, JApA, 42, 17
Burrows, D. N., Hill, J. E., Nousek, J. A., et al. 2005, SSRv, 120, 165
Chamoli, S., Basu, J., Barway, S., et al. 2025, ApJ, 991, 174
Chomiuk, L., Metzger, B. D., & Shen, K. J. 2021, ARA&A, 59, 391
Darnley, M. J. 2021, in The Golden Age of Cataclysmic Variables and Related Objects V (SISSA), 44
Darnley, M. J., Henze, M., Bode, M. F., et al. 2016, ApJ, 833, 149
Darnley, M. J., Hounsell, R., O'Brien, T. J., et al. 2019, Natur, 565, 460
Darnley, M. J., Kuin, N. P. M., & Page, K. L. 2024, ATel, 16752, 1
Evans, A., Banerjee, D. P. K., Geballe, T. R., et al. 2025, MNRAS, 536, 1710
Evans, A., Banerjee, D. P. K., Woodward, C. E., et al. 2023, MNRAS, 522, 4841
Figueira, J., José, J., Cabezón, R., & García-Senz, D. 2025, A&A, 693, A209
Gehrels, N., Chincarini, G., Giommi, P., et al. 2004, ApJ, 611, 1005
Hachisu, I., Kato, M., Kato, T., & Matsumoto, K. 2000, ApJL, 528, L97
Harris, C. R., Millman, K. J., van der Walt, S. J., et al. 2020, Natur, 585, 357
Healy-Kalesh, M. W., Darnley, M. J., Harvey, É. J., et al. 2023, MNRAS, 521, 3004
Healy-Kalesh, M. W., Darnley, M. J., Harvey, É. J., & Newsam, A. M. 2024a, MNRAS, 529, L175
Healy-Kalesh, M. W., Darnley, M. J., Shara, M. M., et al. 2024b, MNRAS, 529, 236
Henze, M., Darnley, M. J., Williams, S. C., et al. 2018, ApJ, 857, 68
Hillman, Y., Prialnik, D., Kovetz, A., & Shara, M. M. 2016, ApJ, 819, 168
Hillman, Y., Shara, M., Prialnik, D., & Kovetz, A. 2020, AdSpR, 66, 1072
Hunter, J. D. 2007, CSE, 9, 90
Kato, M., Saio, H., Hachisu, I., & Nomoto, K. 2014, ApJ, 793, 136
Kemp, A. J., Karakas, A. I., Casey, A. R., et al. 2024, A&A, 689, A222
Kraft, R. P. 1964, ApJ, 139, 457
Krautter, J., Oegelman, H., Starrfield, S., Wichmann, R., & Pfeffermann, E. 1996, ApJ, 456, 788
Kuin, N. P. M., Page, K. L., Mróz, P., et al. 2020, MNRAS, 491, 655
Liller, W. 1990, IAUC, 4961, 2
McKinney, W. 2010, in Proc. 9th Python in Science Conf., ed. S. van der Walt & J. Millman, 56
Mróz, P., Poleski, R., Udalski, A., et al. 2014, MNRAS, 443, 784
Muraoka, K., Kojiguchi, N., Ito, J., et al. 2024, PASJ, 76, 293
Muraoka, K., Kojiguchi, N., Ito, J., et al. 2025, PASJ, 77, 646
Nasa High Energy Astrophysics Science Archive Research Center (Heasarc), 2014 HEAsoft: Unified Release of FTOOLS and XANADU, Astrophysics Source Code Library, ascl:1408.004
Ness, J. U., Beardmore, A. P., Bezak, P., et al. 2022, A&A, 658, A169
Ness, J. U., Beardmore, A. P., Bode, M. F., et al. 2023, A&A, 670, A131
Ness, J. U., Schaefer, B. E., Dobrotka, A., et al. 2012, ApJ, 745, 43
Orio, M., Drake, J. J., Ness, J. U., et al. 2020, ApJ, 895, 80
Osborne, J. P., Page, K. L., Beardmore, A. P., et al. 2011, ApJ, 727, 124
Page, K. L., Kuin, N. P. M., & Darnley, M. J. 2020, ATel, 13731, 1
Pagnotta, A., & Schaefer, B. E. 2014, ApJ, 788, 164
Pagnotta, A., Schaefer, B. E., Clem, J. L., et al. 2015, ApJ, 811, 32
Pojmanski, G. 2002, AcA, 52, 397
Postma, J. E., & Leahy, D. 2021, JApA, 42, 30
Roming, P. W. A., Kennedy, T. E., Mason, K. O., et al. 2005, SSRv, 120, 95
Sala, G., Haberl, F., Schwope, A., et al. 2025, arXiv:2509.08944
Schwarz, G. J., Page, K. L., Kuin, P. M., & Darnley, M. J. 2020, RNAAS, 4, 142
Selvelli, P., & Gilmozzi, R. 2013, A&A, 560, A49
Shafter, A. W., Taguchi, K., Zhao, J., & Hornoch, K. 2022, RNAAS, 6, 241
Shafter, A. W., Zhao, J., Hornoch, K., et al. 2024, RNAAS, 8, 256
Shara, M. M., Lanzetta, K. M., Garland, J. T., et al. 2024a, MNRAS, 529, 224
Shara, M. M., Lanzetta, K. M., Masegian, A., et al. 2024b, ApJL, 977, L48
Shara, M. M., Lanzetta, K. M., Masegian, A., et al. 2025, AJ, 170, 56
Shara, M. M., Prialnik, D., Hillman, Y., & Kovetz, A. 2018, ApJ, 860, 110
Sievers, J. 1970, IBVS, 448, 1
Singh, K. P., Girish, V., Pavana, M., et al. 2021, MNRAS, 501, 36
Singh, K. P., Stewart, G. C., Westergaard, N. J., et al. 2017, JApA, 38, 29
Singh, K. P., Tandon, S. N., Agrawal, P. C., et al. 2014, Proc. SPIE, 9144, 91441S
Starrfield, S., Bose, M., Iliadis, C., et al. 2020, ApJ, 895, 70
Starrfield, S., Iliadis, C., & Hix, W. R. 2016, PASP, 128, 051001
Starrfield, S. G., Sparks, W. M., & Truran, J. W. 1975, MSRSL, 8, 425
Tandon, S. N., Hutchings, J. B., Ghosh, S. K., et al. 2017, JApA, 38, 28
Tandon, S. N., Postma, J., Joseph, P., et al. 2020, AJ, 159, 158
Tody, D. 1993, ASPC, 52, 173
Townsley, D. M., & Bildsten, L. 2004, ApJ, 600, 390
Van Rossum, G., & Drake, F. L. 2009, Python 3 Reference Manual (CreateSpace)
Wang, B. 2018, RAA, 18, 049
Wilms, J., Allen, A., & McCray, R. 2000, ApJ, 542, 914